

Photoprotons from In, Ce, and Bi*

M. E. TOMS AND W. E. STEPHENS
University of Pennsylvania, Philadelphia, Pennsylvania
 (Received June 18, 1953)

The charged particles ejected from indium, cerium, and bismuth foils by x-rays from a 24-Mev betatron were observed in nuclear emulsions. The yields of photoprotons, photodeuterons, and photoalpha particles were determined, and the energy and angular distributions of the photoprotons were measured and compared with theoretical calculations based on the evaporation process and on the direct photoeffect. The energy distributions observed indicate a large fraction of direct photoeffect. A marked forward asymmetry was observed in the angular distributions from indium and bismuth.

INTRODUCTION

THE photodisintegration of medium elements has been shown to consist primarily of a dipole absorption of photons with the subsequent evaporation of a nuclear particle.¹⁻⁶ Nevertheless, several indications suggested that a direct photoeffect is also present.⁵⁻⁸ We have investigated this possibility further by observing the photoprotons from heavier elements, where the yield of evaporation protons is reduced by the Coulomb barrier, thus relatively enhancing other processes. The charged photoparticles ejected by 24-Mev bremsstrahlung x-rays were observed in nuclear emulsions. This made identification of the particles by grain counting possible, as well as measurement of angular and energy distributions. Preliminary results have already been described.⁹ A similar investigation of the photoprotons from Mo¹⁰⁰ and Mo⁹² has been reported

by Butler and Almy¹⁰ and from aluminum and tantalum by Cameron and Hoffman.¹¹

EXPERIMENT

The experimental arrangement is essentially the same as described previously.^{4,6} An improved plate holder was installed in the nuclear emulsion camera to ensure the accurate positioning of the nuclear emulsion plates. Ten $\frac{1}{4}$ -in. \times 1-in. Ilford E-1, 200-micron nuclear emulsion plates were cemented on plate holders at angles of 30°, 50°, 70°, 90°, 110°, to the left and 70°, 90°, 110°, 130°, and 150° to the right of the target foil with their front edges 1.9 cm away from a vertical line through the center of the target. The plane of the surface of the plates was 0.65 cm below the center of the beam. The plates from a single run were developed together by a temperature change method. A double camera was used so that two separate foils could be exposed in each

TABLE I. Exposure details.

Run Foil	Ia In	IIa Bi	IIb Ce	IIIa Bi	IIIb Ba ^a	IVb Ce	Va ...
(mg/cm ²)	18.6	17.5	23	54.7	22.6	28	...
(mils)	1.0	0.8	1.31	2.2	2.36	1.6	...
Betatron energy (Mev)	24	24	24	24	24	23	23
Roentgens at foil	51 800	44 600	37 800	28 400	24 200	23 800	34 000
Emulsion type	E-1	E-1	E-1	E-1	E-1	E-1	C-2
Area scanned (cm ²)	0.396	0.724	0.14	1.37	scanned sideways (62)	0.6	0.32
Total tracks measured	625	116	219	480		584	8
Target half-thickness in Mev for 10-Mev protons	0.2	0.2	0.25	0.5	0.2	0.3	...
Comments		Repeated in IIIa for more intensity	Repeated in IVb as a check				Background

^a Possible oil contamination on foil.

* Aided in part by the Air Research and Development Command and by the joint program of the U. S. Office of Naval Research and the U. S. Atomic Energy Commission.

¹ J. S. Levinger and H. A. Bethe, *Phys. Rev.* **78**, 115 (1950).

² M. Goldhaber and E. Teller, *Phys. Rev.* **74**, 1046 (1948).

³ V. F. Weisskopf and D. H. Ewing, *Phys. Rev.* **57**, 472 (1940).

⁴ M. E. Toms and W. E. Stephens, *Phys. Rev.* **82**, 709 (1951).

⁵ B. C. Diven and G. M. Almy, *Phys. Rev.* **80**, 407 (1950).

⁶ P. R. Byerly, Jr., and W. E. Stephens, *Phys. Rev.* **83**, 54 (1951).

⁷ O. Hirzel and H. Wäffler, *Helv. Phys. Acta* **20**, 373 (1947).

⁸ E. D. Courant, *Phys. Rev.* **82**, 703 (1951).

⁹ M. E. Toms and W. E. Stephens, *Phys. Rev.* **88**, 160 (1952); Stephens, Toms, Carroll, and Rosenblum, *Phys. Rev.* **89**, 893 (1953).

¹⁰ W. A. Butler and G. M. Almy, *Phys. Rev.* **89**, 893 (1953).

¹¹ A. G. W. Cameron and M. M. Hoffman, *Bull. Am. Phys. Soc.* **28**, No. 3, 49 (1953).

run. The details of the various exposures are given in Table I. The first row gives the run number, with the suffix a to indicate the camera nearer to the betatron and b the camera farther from the betatron. The second row gives the element irradiated. The purities of these elements are: Bi 99.9 percent, Ce 98.6 percent, Ba 98 percent, and In 99.9 percent. We can estimate that about 5 to 10 percent of the barium protons might be from the calcium and strontium impurities; for cerium, about 5 percent of the cerium protons may be from iron; and that less than 1 percent of the indium or bismuth protons would be due to impurities. The third and fourth rows show the effective thickness of the foil in milligrams per square cm and in mils. Since the foils were placed at an angle of 30° to the beam, this thickness is greater than the target thickness for the protons emerging normally from the foil. The betatron energy, the roentgen units delivered to the foil, and the emulsion type are given in the next rows. Row eight shows the areas of the emulsion which were

TABLE II. Yield data.

Run Foil	Ia In	IIa Bi	IIb Ce	IIIa Bi	IIIb Ba	IVb Ce	Va ...
Foil width (cm)	1.1	1.1	0.9	0.9	1.1	0.9	...
A (cm ²)	0.292	0.292	0.283	0.240	0.335	0.283	...
$t \times 10^{-3}$ (cm)	5.09	4.06	6.68	11.36	13.4	8.16	...
Protons	623	116	216	475	(62)	556	8
Deuterons	0			4		24	0
Alphas	2		3	1		4	0
$(P/w) \times 10^{-5}$	5.82			1.70		3.50	0.11
$Y_p \times 10^{-4}$	11.7	4	10	5.20	11	12.9	
p/wR	11.2			6.0		11.8	0.32
Estimated background tracks	18			25		16	

scanned, and row nine gives the total tracks observed which fulfilled the criteria of coming from the foil and entering the top surface of the emulsion. The barium plates were scanned perpendicular to the track directions in order to survey the yield. Since there was a possible oil contamination on the surface of the barium foil, these plates were not scanned further. Run IIa for bismuth gave a low yield of protons per field of view and was repeated in run IIIa with a thicker foil. Run IIb with cerium showed a difference between the 90° right and 90° left plate indicating a misalignment. Cerium was therefore repeated in run IVb. In all accepted runs, the 90° right and 90° left plate agreed within the statistical probable error.

Table II gives additional data from which the yields were calculated. The beam did not cover the foils in the horizontal direction. Consequently the area of interception A was calculated from the known geometry. The effective thickness t was calculated from the weight and area of the foils. The sixth, seventh, and eighth rows give the observed protons, deuterons, and alpha particles as identified by grain counting. Alphas

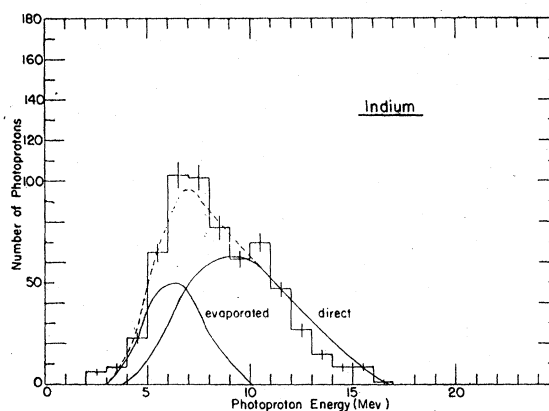


FIG. 1. Histogram of the number of photoprotons observed from indium as a function of proton energy. The calculated curves for the direct and evaporated protons are shown for comparison.

could in general be identified visually. All tracks with a range less than that of a 5-Mev proton were grain-counted in their last 60 microns and compared with the grain counts of recoil protons in the same emulsion. The grain counts in E-1 emulsions scattered more than in C-2 emulsions, and because of the small numbers of deuterons involved the identification was not as clear cut as for the copper photodeuterons.⁶ Row nine gives the numbers of protons per total solid angle corrected for the observed angular distribution. The proton yields are stated in row ten in protons per mole per roentgen unit. Row eleven gives protons per roentgen in order to compare with the background determined in run Va. This is used to estimate the background tracks for runs Ia, IIIa, and IVb as indicated in row twelve. These background tracks are in the energy range from 2.5 to 5 Mev.

Figures 1-3 show the observed energy distributions for indium, cerium, and bismuth. In the indium and bismuth curves, the few tracks identified as alphas or deuterons by grain counting were removed from the

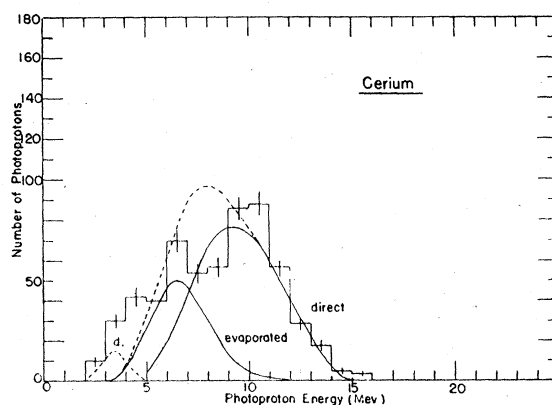


FIG. 2. Histogram of the number of photoprotons observed from cerium as a function of proton energy. The calculated curves for the direct and evaporated protons are shown for comparison. The tracks identified as deuterons are also shown.

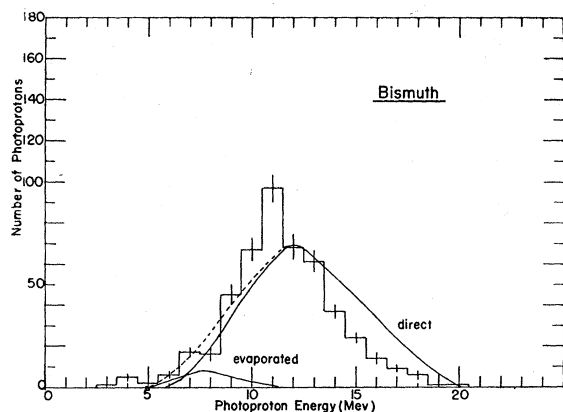


FIG. 3. Histogram of the number of photoprotons observed from bismuth as a function of proton energy. The calculated curves for the direct and evaporated protons are shown for comparison.

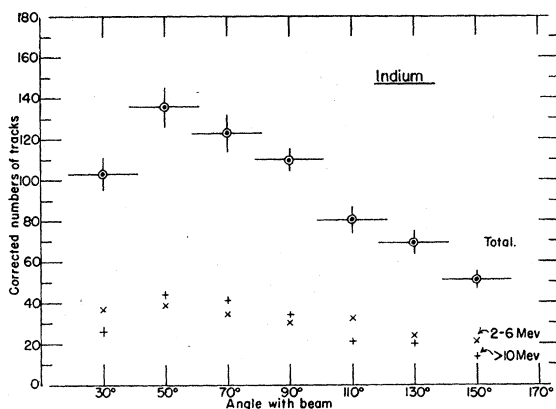


FIG. 4. The angular distribution of the photoprotons from indium. The crosses show the angular distribution of the high-energy and the low-energy protons separately.

energy distribution curve. The deuterons identified from cerium are indicated as a dotted line in the proton energy distribution. These deuterons are plotted against the energy of a proton of the same range as a deuteron. Tracks which passed through the emulsions were grain counted and corrected to their estimated true range. E-1 emulsions were used in all but the background run to reduce fogging due to Compton electrons from the target and thereby permit longer exposures.

Figures 4-6 show the angular distributions observed from indium, cerium, and bismuth. The three sets of points give the total distribution and also the distribution of the low-energy particles and of the high-energy particles. The points for the total distribution are marked with the statistical probable error and the angular spread of observation.

DISCUSSION

The yields of photoparticles corrected for angular distribution and with background subtracted off can be summarized as follows:

bismuth photoprotons	5×10^4 protons mole ⁻¹ r ⁻¹
cerium photoprotons	1.2×10^5 protons mole ⁻¹ r ⁻¹
cerium photodeuterons	6×10^3 deuterons mole ⁻¹ r ⁻¹
cerium photoalphas	8×10^2 alphas mole ⁻¹ r ⁻¹
indium photoprotons	1.1×10^5 protons mole ⁻¹ r ⁻¹

The major uncertainties are in the determination of the solid angles subtended by the emulsions and in the calibration of the x-ray beam. It is estimated that the uncertainty in the proton yields is of the order of 20 percent. There is additional uncertainty in the deuteron and alpha yields due to identification uncertainty and statistical fluctuations. The barium yield in Table II is only an estimate subject to possible contamination errors and poor statistics.

Mann and Halpern¹² give a photoproton yield from indium of 1.3×10^5 protons mole⁻¹ r⁻¹ as determined by a ZnS scintillation detector.

In order to compare these results with theoretical values, we have made calculations using both the

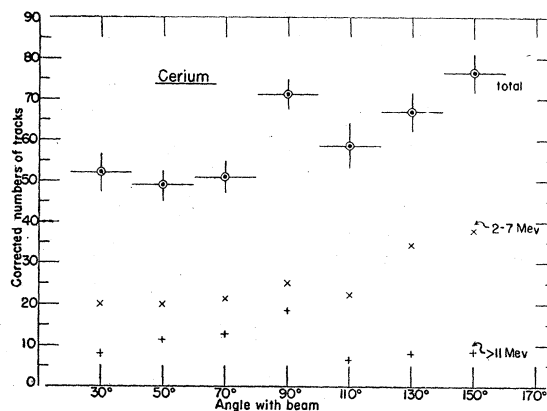


FIG. 5. The angular distribution of the photoprotons from cerium. The crosses show the angular distribution of the high-energy and the low-energy protons separately.

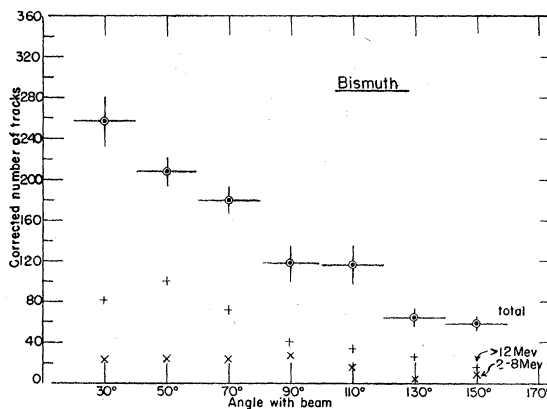


FIG. 6. The angular distribution of the photoprotons from bismuth. The crosses show the angular distribution of the high-energy and the low-energy protons separately.

¹² A. K. Mann and J. Halpern, Phys. Rev. 82, 733 (1951).

evaporation process³ of emission and the direct photoeffect.⁸ In each case the charged particle yields are determined by the bremsstrahlung spectrum, the photon absorption, the binding energies, and the Coulomb barrier. The pertinent binding energies for the nuclei involved are given in Table III. In each element the values for the dominant isotope were used. The bremsstrahlung distribution was calculated from Schiff's¹³ formula as adapted by Johns *et al.*¹⁴ The photon absorption curves are not known but are presumed to be well approximated by the (γ, n) cross section curves. $\text{Bi}(\gamma, n)$ is given by Halpern, Nathans, and Mann¹⁵ while the Ce and In curves were adapted from the $\text{Ta}(\gamma, n)$ curve¹⁶ normalized to the neutron yield data of Price and Kerst¹⁷ corrected by the multiplicity factor of Heidmann and Bethe.¹⁸ The Coulomb penetration factors are taken from Weisskopf's tables¹⁹ using $r_0 = 1.5 \times 10^{-13}$ cm or $r_0 = 1.3 \times 10^{-13}$ cm.

In calculating the photoproton yields to be expected on the evaporation model, it is simple and direct to determine the ratio of the (γ, p) cross section to the (γ, n) cross section from the F functions defined by Blatt and Weisskopf¹⁹ (page 369). Using the binding energies given in our Table III, the excitation energies were determined for various photon energies. The corresponding F_n and F_p were read off the curves²⁰ for $r_0 = 1.5 \times 10^{-13}$ cm and their ratio weighted by the bremsstrahlung distribution and photon absorption values. The resulting theoretical $(\gamma, p)/(\gamma, n)$ ratios are 1.3×10^{-3} , 8×10^{-5} , 6×10^{-5} , and 6×10^{-4} for indium, barium, cerium, and bismuth. The ratios for $r_0 = 1.3 \times 10^{-13}$ cm or for older penetration factors give even smaller values. Photon neutron yields¹⁷ of 0.9×10^7 , 1.1×10^7 , 1.2×10^7 , and 2.5×10^7 neutrons per mole per roentgen units combine with our photoproton yields of 1.1×10^5 , 1×10^5 , 1.2×10^5 , and 0.5×10^5 protons per mole per r for indium, barium, cerium and bismuth to give observed $(\gamma, p)/(\gamma, n)$ ratios of 1.2×10^{-2} , 1×10^{-2} , 1×10^{-2} , and 0.2×10^{-2} , respectively. In every case the observed ratio is higher than the calculated.

These results confirm and extend the results of Waffler,⁷ who measured the radioactivity produced by some (γ, p) reactions induced by monochromatic gamma rays. Although the F functions are not very well known (especially for even- A isotopes), such results imply some marked departure from the evaporation process. In order to further elucidate these discrepancies, we have calculated the energy distributions to be expected from evaporated and direct photoprocesses.

¹³ L. I. Schiff, Phys. Rev. **83**, 252 (1951).

¹⁴ Johns, Katz, Douglas, and Haslam, Phys. Rev. **80**, 1062 (1950).

¹⁵ Halpern, Nathans, and Mann, Phys. Rev. **88**, 679 (1952).

¹⁶ L. Katz and A. G. W. Cameron, Can. J. Phys. **29**, 518 (1951).

¹⁷ G. A. Price and D. W. Kerst, Phys. Rev. **77**, 806 (1950).

¹⁸ J. Heidmann and H. A. Bethe, Phys. Rev. **84**, 274 (1951).

¹⁹ J. M. Blatt and V. Weisskopf, *Theoretical Nuclear Physics* (John Wiley and Sons, Inc., New York, 1952), pp. 352.

²⁰ Fast Neutron Data, Atomic Energy Commission Report NYO-632, 1950 (unpublished).

TABLE III. Binding energies.^a

Z	Element	A	Abundance	B_n (MeV)	B_p (MeV)	B_d (MeV)	B_α (MeV)
49	In	113	0.04	9.4	6.1	12.9	2.1
		115	0.96	9.05 ^b	6.8	13.1	2.5
56	Ba	138	0.72	7.5	9.6	14.7	2.3
58	Ce	140	0.89	9.05 ^b	8.5	14.1	1.2
		142	0.11	7.15 ^b	9.1	14.3	1.6
83	Bi	209	1.00	7.44 ^c	3.76 ^d	10.4	-3.15 ^e

^a N. Metropolis and G. G. Reitwiesner, *Tables of Atomic Masses*, U. S. Atomic Energy Commission Report NP 1980, 1950 (unpublished).

^b Sher, Halpern, and Mann, Phys. Rev. **84**, 387 (1951).

^c J. A. Harvey, Phys. Rev. **81**, 353 (1951).

^d K. Way (private communication).

^e H. Faraggi and A. Berthelot, Compt. rend. **232**, 2093 (1951).

TABLE IV. Direct and evaporation yields of photoprotons (particles per mole per roentgen unit).

	In	Ce	Bi
Observed direct	8×10^4	9×10^4	5×10^4
evaporation	3.5×10^4	4×10^4	0.3×10^4
Theoretical direct	2×10^4	0.7×10^4	1.5×10^4
evaporation	1.1×10^4	0.07×10^4	0.3×10^4

The energy distribution of the photoprotons evaporated from a compound nucleus can be calculated as described before.⁶ Here we have used the level density from a statistical model: $W(E) = C \exp(2(aE)^{1/2})$, where C and a are given in the Fast Neutron Data report.²⁰ The relative energy distributions calculated were matched to the experimental curves as in Figs. 1-3 and the "observed-evaporation" partial yields so determined are tabulated in Table IV. The evaporation calculated yields are also given in Table IV. In addition, the evaporation yields of deuterons and alpha particles were similarly calculated to be: 100 alphas mole⁻¹ r⁻¹ and 2 deuterons mole⁻¹ r⁻¹ for bismuth. These are to be compared with the very approximate observed values of 200 alphas mole⁻¹ r⁻¹ and 400 deuterons mole⁻¹ r⁻¹. The calculated yield for bismuth, given as 0.3×10^4 protons mole⁻¹ r⁻¹, is for $r_0 = 1.3 \times 10^{-13}$ cm. The bismuth yield for $r_0 = 1.5 \times 10^{-13}$ cm would be calculated to be 1.3×10^4 protons mole⁻¹ r⁻¹. For cerium and indium, on the other hand, the nuclear radius seems to favor $r_0 = 1.5 \times 10^{-13}$ cm and so the calculated evaporated yields are based on $r_0 = 1.5 \times 10^{-13}$ cm. In comparing the observed energy distributions to those expected from evaporated protons, it is evident that a large number of the photoprotons have energies greater than calculated. The calculated yields of evaporated protons for indium and bismuth is at least consistent with a portion of the observed particles. However, in cerium, the evaporated yield is so depressed by the large proton binding energy that practically no evaporated protons should be observed.

It is interesting, then, to calculate the energy distribution and yield of photons to be expected from a

direct photoeffect. Courant's⁸ formula has been extended to allow a determination of the energy distribution by simplifying its dependence on photon energy and rearranging it to give

$$y(\epsilon) \approx (Z^2/4A^{4/3})aF(\epsilon) \int_{E_{\min}}^{E_{\max}} (N_\gamma(E)/E^3)dE,$$

where $y(\epsilon)$ is the number of protons of energy ϵ per mole per r ejected by a beam of photons of energy distribution $N_\gamma(E)$ with a maximum energy E_{\max} and $E_{\min} = \epsilon + B_p$ (B_p is the proton binding energy); a is Avogadro's number and $F(\epsilon)$ is the Coulomb barrier penetration cross section. The total yield can be determined more directly by

$$Y = (34.3aZ^2/A^{4/3}) \int_{B_p}^{E_{\max}} \left[(N_\gamma(E)/E^3) \int_0^{x_1} F(x)dx \right] dE,$$

where $x_1 = (E_{\max} - B_p)/C_B$ (C_B is Coulomb barrier height). Using these relations, the curves marked "direct" in Figs. 1-3 were calculated and the direct yields given in Table IV were determined. Again the relative energy distribution curves were matched to the observed histograms, and the yields so deduced are given in Table IV as "observed-direct" protons. Since Courant's formulation is quite approximate, the agreement in the case of indium is regarded as excellent. For bismuth the yield is in good agreement, but the calculated energy distribution is somewhat too high in energy. The cerium calculated yield is low by a factor of 10 although the energy distribution is in reasonable agreement. Nevertheless, in every case the interpretation of appreciable direct photoprotons is evident.

The observed angular distribution of the photoprotons show rather striking anisotropies. Indium and especially bismuth show a large forward asymmetry. This is rather unexpected, since evaporated protons should be essentially isotropic and direct photoeffect

protons should have a distribution of the form $A + B \sin^2\theta$, where the rate of A to B depends on the proton angular momentum⁸ (assuming dipole absorption). Each of these effects is symmetric about 90° . The photon momentum is not large enough to affect this symmetry. Several explanations can be considered for the observed effects. An asymmetry can be caused by a dipole-quadrupole interference effect²¹ producing an angular distribution of the form $I(\theta) = a + b(\sin\theta + p \sin\theta \cos\theta)^2$, where a is an isotropic component (evaporated protons), and b is the asymmetric component (direct protons) with $p^2/5 = \sigma_q/\sigma_d$, the ratio of the electric quadrupole to electric dipole absorption cross sections. The total photoprotons from indium shown in Fig. 4 can be fitted by an angular distribution of this type, with p between $\frac{3}{4}$ and 1 together with $b/a = 0.85$ to 0.95 . The total photoprotons from bismuth shown in Fig. 6 have an excess of protons at 30° which cannot be fitted by a curve of this type. The bismuth photoprotons of greater than 10 Mev can, however, be fitted with this type of angular distribution with a p of approximately 2 and a b/a about $\frac{3}{2}$. The cerium photoprotons, on the other hand, show no evidence of such an effect.

Schiff²² has suggested (on the assumption of virtual deuterons in the nucleus) that a forward asymmetry will result from the variation in cross section of the deuteron photoeffect, depending on the approach or recession of the deuteron relative to the photon.

We wish to acknowledge with gratitude discussions with Dr. Arnold Feingold and Dr. Sherman Frankel, which have contributed to our calculations of the direct photoeffect, the aid of E. E. Carroll, Jr. in scanning the indium plates, and the help of the late G. K. Rosenblum in some of the photoeffect calculations.

²¹ Mann, Halpern, and Rothman, Phys. Rev. **87**, 146 (1952); L. I. Schiff, Phys. Rev. **78**, 733 (1950); J. F. Marshall and E. Guth, Phys. Rev. **78**, 738 (1950); J. S. Levinger, Phys. Rev. **84**, 43 (1951).

²² L. I. Schiff (private communication).